ACS ENGINEERING Au
AN OPEN ACCESS JOURNAL OF THE AMERICAN CHEMICAL SOCIETY

pubs.acs.org/engineeringau
Article

Hierarchical Computational Screening of Quantum Metal−Organic Framework Database to Identify Metal−Organic Frameworks for Volatile Organic-Compound Capture from Air

Published as part of the ACS Engineering Au virtual special issue "Materials Design".

Goktug Ercakir, Gokhan Onder Aksu, Cigdem Altintas, and Seda Keskin*

Cite This: ACS Eng. Au 2023, 3, 488−497
Read Online

ABSTRACT: The design and discovery of novel porous materials that can efficiently capture volatile organic compounds (VOCs) from air are critical to address one of the most important challenges of our world, air pollution. In this work, we studied a recently introduced metal−organic framework (MOF) database, namely, quantum MOF (QMOF) database, to unlock the potential of both experimentally synthesized and hypothetically generated structures for adsorption-based *n*-butane (C_4H_{10}) capture from air. Configurational Bias Monte Carlo (CBMC) simulations were used to study the adsorption of a quaternary gas mixture of N_2, O_2, Ar, and C_4H_{10} in QMOFs for two different processes, pressure swing adsorption (PSA) and vacuum-swing adsorption (VSA). Several adsorbent performance evaluation metrics, such as C_4H_{10} selectivity, working capacity, the adsorbent performance score, and percent regenerability, were used to identify the best adsorbent candidates, which were then further studied by molecular simulations for C_4H_{10} capture from a more realistic seven-component air mixture consisting of N_2, O_2, Ar, C_4H_{10}, C_3H_8, C_3H_6, and C_2H_6. Results showed that the top five QMOFs have C_4H_{10} selectivities between 6.3×10^3 and 9×10^3 (3.8×10^3 and 5×10^3) at 1 bar (10 bar). Detailed analysis of the structure−performance relations showed that low/mediocre porosity (0.4−0.6) and narrow pore sizes (6−9 Å) of QMOFs lead to high C_4H_{10} selectivities. Radial distribution function analyses of the top materials revealed that C_4H_{10} molecules tend to confine close to the organic parts of MOFs. Our results provided the first information in the literature about the VOC capture potential of a large variety and number of MOFs, which will be useful to direct the experimental efforts to the most promising adsorbent materials for C_4H_{10} capture from air.

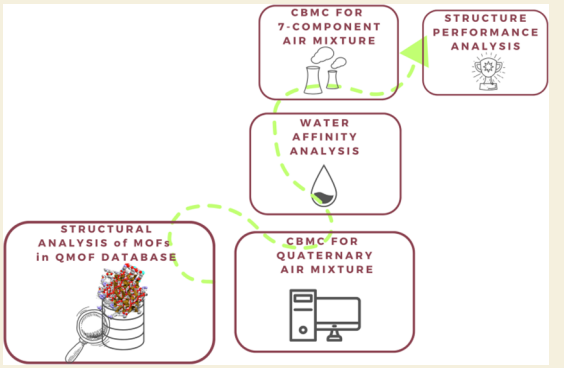

KEYWORDS: *metal−organic framework (MOF), volatile organic compounds (VOCs), adsorption, selectivity, molecular simulation*

1. INTRODUCTION

Along with the growth in the industrial production, the increase of volatile organic compound (VOC) emissions in the atmosphere, even in trace amounts, poses a significant threat to human and environmental health.[1−3] While oxidation, biofiltration, and catalytic methods are commonly utilized to address VOC-based air pollution, these approaches have limitations such as secondary pollution, cost-effectiveness, and low energy efficiency.[4,5] Adsorption-based separation of VOCs from air using novel porous materials offers an environmentally friendly and energy-efficient solution.[6] A large variety of porous materials, such as activated carbons and zeolites, have been widely used for VOC capture to date.[6] A unique class of porous materials, namely, metal−organic frameworks (MOFs), has recently emerged as very strong candidates to traditional porous materials for the adsorption of a large variety of gas molecules. MOFs, which are composed of metal nodes and organic linkers, have distinct advantages such as tunable physicochemical properties, record surface areas, tailorable pore sizes, and ultrahigh porosities.[6−8] Owing to these features, they have been widely studied for selective gas capture, mostly for CO_2 separation from CH_4, N_2, and air.[9−11] MOFs have also been widely investigated for air pollution control as discussed in several reviews.[7,10] Early promising results accelerated the efforts toward the design of new MOFs, leading to a continuous increase in the number of synthesized MOFs, which already exceeded hundreds of thousands of distinct materials. However, studying thousands of MOFs

Received: August 7, 2023
Revised: September 22, 2023
Accepted: September 22, 2023
Published: October 7, 2023

using purely experimental methods is not feasible due to time and resource limitations.

Molecular simulations have been very useful to assess the performance of MOFs for a target application to direct experimental efforts to the most promising materials and to complement experimental studies by providing molecular-level insights into the materials' structure−performance relations. For capturing VOCs using MOFs, Severino et al.[12] utilized Grand Canonical Monte Carlo (GCMC) simulations to reveal the adsorption mechanism of acetic acid inside functionalized MIL-53(Al). GCMC simulations were used to determine the adsorption sites of the VOCs benzene (C_6H_6) and toluene ($C_6H_5CH_3$) in a MOF decorated with acidic and basic groups.[13] González-Galán et al.[14] combined GCMC simulations with breakthrough experiments to investigate the performance of TAMOF-1 for various VOC separations and also reported *o*-xylene/*m*-xylene selectivities of up to ∼2.5 at 393 K and benzene/cyclohexane selectivity of up to 8 at 298 K.

Development of experimental and hypothetical MOF (hMOF) databases such as the Cambridge Structural Database (CSD, 121,093 MOFs),[15,16] Computation-Ready and Experimental MOF database (CoRE MOF, 14,142 MOFs),[17,18] Boyd's database (BW-DB, 325,000 hMOFs),[19,20] Genomic MOF database (GMOF, 303,991 hMOFs),[21] and Topologically Based Crystal Constructor database (ToBaCCo, 13,512 hMOFs)[22] accelerated the high-throughput computational screening (HTCS) studies that have generally focused on CH_4 and H_2 storage and CO_2 capture.[23−26] While numerous molecular simulation studies screened these databases for adsorption-based separation of gas mixtures,[27,28] research focusing on VOC capture remains very limited. Gulcay-Ozcan et al.[29] examined the toluene capture performance of 459 CoRE MOFs using continuous-fractional component Monte Carlo (CFCMC) simulations, computed toluene uptakes up to 8 mmol/g, and toluene selectivities in the range of 10^3−10^8 for the separation of $C_6H_5CH_3/N_2/O_2$ mixtures at 1 bar and 298 K. Small pore sizes (between 6 and 10 Å), high accessible surface areas (>1,600 m^2/g), and high porosities (>0.6) were found to be the common properties of the promising MOFs with high $C_6H_5CH_3$ selectivity. Liu et al.[30] performed GCMC simulations to compute $C_6H_5CH_3$ adsorption capacities of 2,500 CoRE MOFs at 1,900 Pa and 298 K, revealing that 802 MOFs exhibited higher $C_6H_5CH_3$ adsorption capacities compared to the promising MOF, HKUST-1 (6.34 mmol/g). Top MOFs with the highest $C_6H_5CH_3$ adsorption capacities tend to have high gravimetric surface areas (>4,600 m^2/g) and void fractions (>0.8). Yuan et al.[31] screened 2,179 hMOFs by performing GCMC simulations at 1 bar, 298 K for capturing formaldehyde (HCHO) from air and computed HCHO selectivities of hMOFs up to 1.2×10^3 as hMOFs with pore sizes of ∼5 Å offered high selectivities. The same group followed a similar approach using GCMC simulations to assess the potential of 31,399 hMOFs in capturing C_3−C_4 alkanes from an air mixture mimicking $VOC/N_2/O_2$ and calculated propane (C_3H_8) selectivities between 10^{-3} and 7.3×10^5 and butane (C_4H_{10}) selectivities between 0.1 and 5.7×10^6 at 1 bar and 298 K.[32]

The hybrid quantum-MOF database (QMOF, 20,375 MOFs),[33,34] which consists of experimental and hypothetical computation-ready MOFs collected from previously mentioned databases, has been recently introduced to offer a diverse collection of structurally optimized structures with a comprehensive range of chemical and physical properties.[22] This database was studied for predicting several properties of MOFs such as band gaps[33,35] and heat capacities,[36] but it has not been screened for a gas separation application to the best of our knowledge. Motivated by this, we aimed to screen this diverse material space for VOC capture and unlock the potential of QMOFs for adsorption-based C_4H_{10} separation from air for the first time in the literature. A total of 3,496 structurally optimized QMOFs were studied for two different adsorption-based processes, vacuum swing adsorption (VSA), and pressure swing adsorption (PSA). We mimicked air as a quaternary gas mixture consisting of N_2, O_2, Ar, and C_4H_{10} and performed configurational bias Monte Carlo (CBMC) simulations to compute several adsorbent performance evaluation metrics of MOFs including the selectivity, working capacity, adsorbent performance score, and percent regenerability. The most promising materials identified based on these metrics were further examined for C_4H_{10} separation from a more realistic seven-component air mixture composed of N_2, O_2, Ar, C_4H_{10}, C_3H_8, propene (C_3H_6), and ethane (C_2H_6). The high-performing materials identified under VSA and PSA conditions were studied in detail to understand the impact of their structural and chemical properties, such as linker subunits and metal types on their gas adsorption performances by performing radial distribution function (RDF) analyses. Computational screening of this recent hybrid MOF database for VOC capture and generation of structure-performance relations for high-performing materials will provide valuable molecular insights into the rational design of new materials that will address one of the most important challenges of the world, namely, air pollution.

2. COMPUTATIONAL DETAILS

Figure 1 represents the computational methodology that we proposed to study MOF adsorbents for direct VOC capture from air. Crystallographic structures of MOFs, which were relaxed and optimized by density functional theory (DFT) calculations, were obtained from the QMOF database.[33,34] The QMOF database consists of 20,375 different types of non-disordered, unbounded solvent-free structures where 16,884 MOFs are synthesized and 3,491 of them are hypothetical. Structural features of all QMOFs, such as the accessible surface area (S_{acc}), porosity (ϕ), largest cavity diameter (LCD), and pore limiting diameter (PLD), were calculated using Zeo++ software (version 0.3).[37] A probe diameter of 3.72 Å representing the N_2 molecule was used to compute the surface area, whereas a zero probe was used for the geometric pore volume calculations. We focused on the QMOFs having PLDs greater than the kinetic diameter of the largest molecule in our air mixture (C_3H_8, 5 Å)[38,39] and ended up with 3,496 materials, including 671 experimentally synthesized and 2,825 hypothetical QMOFs.

Configurational bias Monte Carlo (CBMC)[40] simulations were performed using the RASPA[41] simulation package to compute the adsorption of a 4-component air mixture (77.922% N_2, 20.979% O_2, 0.999% Ar, and 0.1% C_4H_{10}) in QMOFs. This composition was set to represent an ambient air mixture with trace amounts of VOCs.[42] In order to determine the number of cycles required for our CBMC simulations, we compared the gas uptakes of 100 QMOFs acquired by a total of 10^6 and 10^5 simulation cycles. Figure S1 shows that the simulation results obtained with 10^6 and 10^5 cycles for the uptakes of N_2, O_2, Ar, and C_4H_{10} in QMOFs are very close.

https://doi.org/10.1021/acsengineeringau.3c00039
ACS Eng. Au 2023, 3, 488−497

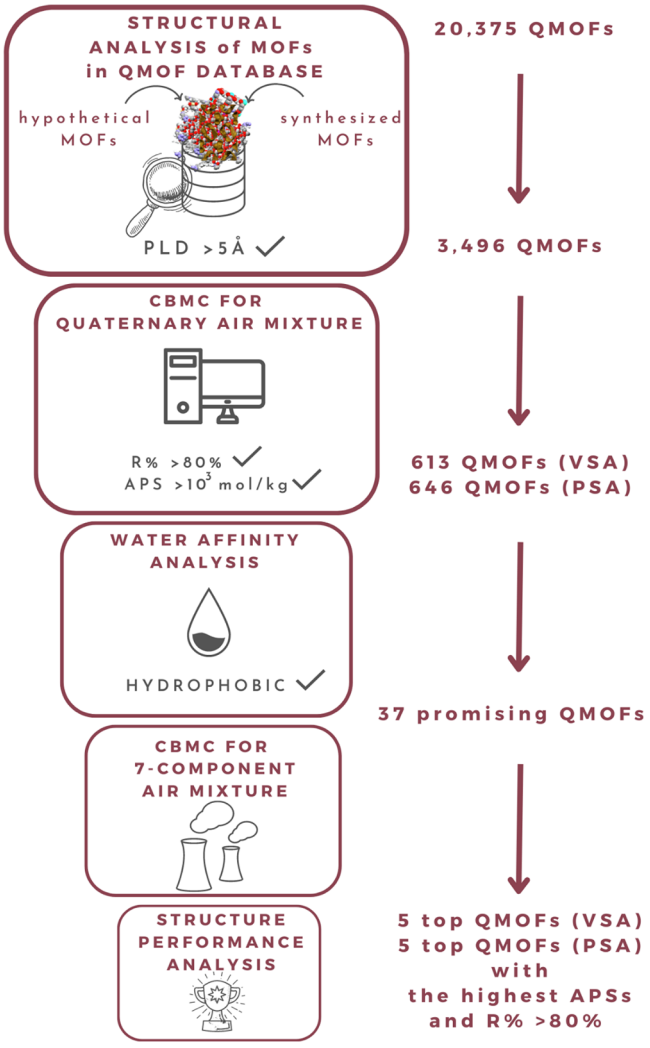

Figure 1. Hierarchical computational screening methodology used in this work.

Therefore, a total of 10^5 cycles were found to be sufficient to avoid excessive usage of the computational time. Transferable potentials for phase equilibria (TraPPE) force field was used for all gas models, that is, C_4H_{10}, C_3H_8, C_3H_6, C_2H_6, N_2, and O_2.[43] All VOCs (C_4H_{10}, C_3H_8, C_3H_6, and C_2H_6) were modeled as flexible molecules.[43] N_2 and O_2 were modeled using rigid, three-site models, including one site at the center of the molecule and one site on each side of the molecule.[44−46] Ar was modeled as a single Lennard-Jones (LJ) site.[47] Dreiding[48] force field was used for QMOFs, and parameters of metals that are not available in Dreiding were taken from the Universal Force Field (UFF).[49] LJ 12−6 interactions were considered for all gas molecules, while Coulombic interactions were considered only for N_2 and O_2. The cross-interaction parameters were obtained using the Lorentz−Berthelot mixing rule. The Coulombic interactions for N_2 and O_2 were calculated using the Ewald summation.[50] Density-derived electrostatic and chemical (DDEC6)[51,52] point charges available in the QMOF database were used to compute the Coulombic interactions. A cutoff distance of 12 Å was used for the LJ interactions, and simulation boxes were ensured to have at least twice the specified cutoff distance in each direction. The coordinates of all framework atoms were frozen to save computational time following the literature.[53]

Simulations were performed mimicking PSA (adsorption pressure: 10 bar; desorption pressure: 1 bar) and VSA (adsorption pressure: 1 bar; desorption pressure: 0.1 bar) processes at 298 K. A Peng−Robinson equation of state was used to convert the fugacity to pressure. Figure S2a shows the good agreement between our simulation results performed using these parameters and the results of previous works, which reported single-component C_4H_{10} uptakes in three MOFs, namely, IRMOF-1[54] (at 300 K), Cu-BTC[55] (at 298 K), and ZIF-8[56] (at 273 K), at 0.1, 1, and 10 bar. Our simulation results for equimolar C_4H_{10}/C_4H_8 and C_3H_8/C_3H_6 mixture adsorption in Cu-BTC were also shown to be in a good agreement with the previously reported values[55] in Figure S2b at various pressures at 298 K, suggesting that our computational methodology is valid.

Gas uptakes obtained from the results of molecular simulations for the four-component (quaternary) mixture adsorption were used to compute several adsorbent performance evaluation metrics such as the adsorption selectivity ($S_{C4H10,quat}$), working capacity ($\Delta N_{C4H10,quat}$), adsorbent performance score ($APS_{C4H10,quat}$), and percent regenerability ($R\%_{C4H10,quat}$) of QMOFs for the selective capture of C_4H_{10} from air. The selectivity of QMOFs for the separation of C_4H_{10} was calculated as follows: $S_{C4H10,quat} = (N_{C_4H_{10}}/(N_{O_2} + N_{Ar} + N_{N_2}))/(y_{C_4H_{10}}/(y_{O_2} + y_{Ar} + y_{N_2}))$ where N_i and y_i demonstrate the adsorbed gas amount and the mole fraction for gas species i in the bulk mixture, respectively. The working capacity was defined as the difference between the adsorbed amounts of C_4H_{10} at adsorption and desorption pressures, $\Delta N_{C4H10,quat} = N_{ads,\ C_4H_{10}} - N_{des,\ C_4H_{10}}$. The adsorbent performance score $APS_{C4H10,quat}$ was described as the product of $\Delta N_{C4H10,quat}$ and $S_{C4H10,quat}$ at the adsorption pressure. The percent regenerability ($R\%_{C4H10,quat}$) was calculated as the ratio of $\Delta N_{C4H10,quat}$ to $N_{C4H10,quat}$. Adsorbents offering high selectivity, high working capacity, and high regenerability are desired for an efficient gas separation process. Therefore, we focused on the materials offering $R\%_{C4H10,quat}$ > 80% and $APS_{C4H10,quat}$ > 10^3 mol/kg and identified a total of 1,182 MOFs (536 QMOFs at VSA condition, 569 QMOFs at PSA condition, and 77 common QMOFs of VSA and PSA conditions) for further examination.

Water vapor (H_2O) might also be present in the VOC-including air mixtures, and there might be competitive adsorption between C_4H_{10} and H_2O, which may adversely affect the C_4H_{10} separation performance of MOFs.[28,32] Therefore, potentially promising 1,182 QMOFs identified in the previous step were further filtered to focus on presumably hydrophobic structures. We used the Henry's constant of H_2O ($K_{H,H2O}$) for a well-known hydrophobic MOF, namely, ZIF-8, as a criterion.[57] To compute $K_{H,H2O}$ values of QMOFs, Widom insertion simulations were performed at 298 K with 10^6 cycles using RASPA,[41] where a five-site TIP5P/2018[58] model was used for H_2O. Based on the reference $K_{H,H2O}$ value computed for ZIF-8 (2.5×10^{-6} mmol/g/Pa), 37 hydrophobic QMOFs having a $K_{H,H2O} < 2.5 \times 10^{-6}$ mmol/g/Pa, a $R\%_{C4H10,quat}$ > 80%, and the highest $APS_{C4H10,quat}$ were selected among 1,182 QMOFs. These 37 promising QMOFs were then studied for the adsorption of a more realistic seven-component air mixture (77.922% N_2, 20.979% O_2, 0.999% Ar, 0.025% C_4H_{10}, 0.025% C_3H_8, 0.025% C_3H_6, and 0.025% C_2H_6)[59−61] both at VSA and PSA conditions. In this case, 10^5 initialization and 10^5 production cycles were employed during the CBMC

https://doi.org/10.1021/acsengineeringau.3c00039
ACS Eng. Au 2023, 3, 488−497

simulations. The selectivity of QMOFs for separating C_4H_{10} from the seven-component air mixture was calculated using the formula $S_{C4H10,7\text{-comp}} = (N_{C_4H_{10}}/(N_{O_2} + N_{Ar} + N_{N_2}+N_{C_3H_8} + N_{C_3H_6} + N_{C_2H_6}))/(y_{C_4H_{10}}/(y_{O_2} + y_{Ar} + y_{N_2} + y_{C_3H_8} + y_{C_3H_6} + y_{C_2H_6}))$.

Other adsorbent performance metrics, namely, the $APS_{C4H10,7\text{-comp}}$, $\Delta N_{C4H10,7\text{-comp}}$, and $R\%_{C4H10,7\text{-comp}}$, were calculated using their corresponding definitions given above but using the gas uptakes obtained from the simulations for the seven-component air mixture.

The top five QMOFs that exhibit the highest $APS_{C4H10,7\text{-comp}}$ with $R\%_{C4H10,7\text{-comp}} > 80\%$ were identified separately for VSA and PSA processes, and their structural and chemical properties were examined in detail to understand what types of features are important to obtain high-performing adsorbents for VOC capture. We utilized MOFseek software version 1.0[62] for linker subunit and metal-type analyses of the high-performing QMOFs. Functional groups connected to the linkers were first removed to obtain linker subunits, and six different types of linker subunits were identified, as listed in Table S1. We also retrieved information from the QMOF database regarding the metal node information, topology of structures, and whether the QMOFs are hypothetical or synthesized.[33,34] To better understand the gas adsorption behavior, RDF analyses were performed for the top 2 materials, in addition to the visualization of the snapshots taken from the CBMC simulations showing the distribution of gas molecules in the framework during adsorption obtained via Mercury software.[63]

3. RESULTS AND DISCUSSION

Figure 2 represents the performance of QMOFs for the adsorption-based separation of a quaternary air mixture under PSA and VSA conditions. Figure 2a shows that C_4H_{10} selectivities ($S_{C4H10,quat}$) of hypothetical QMOFs at 1 bar are ranging from 2.6 to 1.8×10^5 and their working capacities $\Delta N_{C4H10,quat}$ vary from 1×10^{-3} to 4.6 mol/kg at VSA conditions. Many synthesized QMOFs were computed to have higher selectivities, that is, $18-4.2 \times 10^5$, and similar working capacities, that is, 3.2×10^{-3} to 3.9 mol/kg, compared to the hypothetical QMOFs, as shown in Figure 2b. The butane separation performance of hypothetical and synthesized QMOFs at PSA condition are shown in Figure 2c,d. Butane working capacities of hypothetical and synthesized QMOFs were computed as $0.01-6.8$ and 7.4×10^{-3} to 5.3 mol/kg under PSA condition, respectively, which are higher than the values obtained under VSA condition. Butane selectivities of adsorbents at 10 bar vary in a large range, that is, between 3.1 and 5.2×10^4 and $20-1.3 \times 10^5$ for hypothetical and synthesized QMOFs, respectively, indicating that the large chemical and structural diversity of this material space results in wide varieties in their separation potentials. We note that the QMOFs with very high selectivities suffer from low working capacities. For example, 15 QMOFs offering selectivities of $>10^5$ at VSA condition have working capacities in the range of $0.05-0.37$ mol/kg as shown in Figure 2a,b and 128 QMOFs having selectivities of $>10^4$ at PSA condition offer working capacities between 7.4×10^{-3} and 0.71 mol/kg in Figure 2c,d.

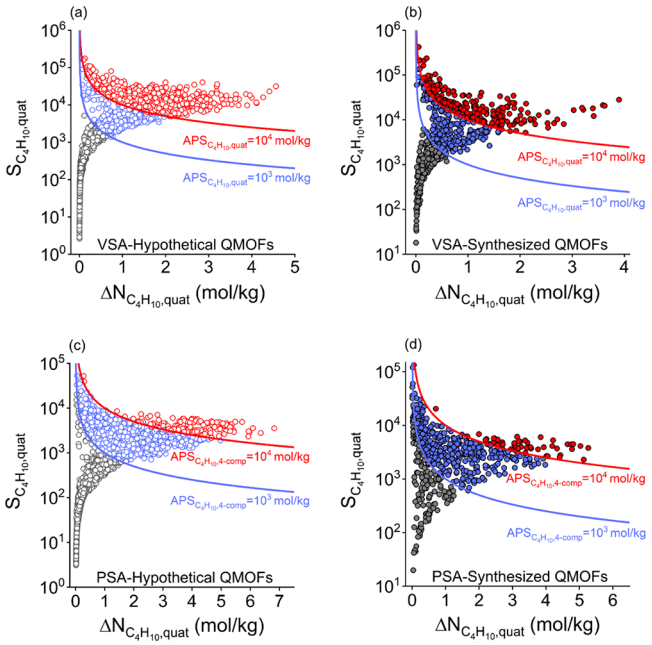

Figure 2. Selectivities and working capacities of hypothetical and synthesized QMOFs calculated for the separation of C_4H_{10} from the quaternary air mixture at (a, b) VSA and (c, d) PSA conditions.

In Figure 2, gray data points show the QMOFs with $APS_{C4H10,quat} < 10^3$ mol/kg, which are potentially unpromising adsorbents suffering from either low selectivity or low working capacity, while blue data points show QMOFs having $10^3 < APS_{C4H10,quat} < 10^4$ mol/kg with mediocre performance. Red data points represent the QMOFs offering the highest $APS_{C4H10,quat}$ ($>10^4$ mol/kg), which generally provide a combination of high selectivity and high working capacity. At VSA (PSA) condition, 221 (54) synthesized and 410 (172) hypothetical QMOFs have $APS_{C4H10,quat} > 10^4$ mol/kg. Although working capacity values are lower at VSA condition, the number of QMOFs with $APS_{C4H10,quat} > 10^4$ mol/kg is higher compared to those at PSA conditions, which signals that $S_{C4H10,quat}$ has a more pronounced effect in determining the $APS_{C4H10,quat}$ at VSA conditions. We also compared the separation performance of QMOFs with commercial zeolite MFI. To have a more balanced comparison, we computed the selectivity of MFI for the separation of C_4H_{10} from a quaternary air mixture (1.3×10^3 at 1 bar and 1.4×10^3 at 10 bar, 298 K) using the reported gas uptakes for the separation of the same quaternary air mixture.[42] We concluded that more than one-third of 3,496 QMOFs (1,403 QMOFs at 1 bar and 1,514 QMOFs at 10 bar) have higher C_4H_{10} selectivities than MFI. This highlights the significant potential of utilizing MOFs for adsorption-based C_4H_{10} separation from air.

To identify high-performing adsorbents, we used $APS_{C4H10,quat}$ as the main performance metric; however, many other metrics also exist. For example, trade-off between the selectivity and uptake (TSN),[28] which is the product of the gas uptake and logarithm of selectivity, was proposed to determine whether a material has both high selectivity and high uptake. We computed the TSN values of all QMOFs for VSA and PSA processes and compared the rankings of materials based on TSN with the rankings based on $APS_{C4H10,quat}$. Results showed that 959 (831) of the QMOFs are common in the first 1,000 MOFs with the highest APS and TSN at VSA (PSA) conditions, indicating that either one of

https://doi.org/10.1021/acsengineeringau.3c00039
ACS Eng. Au 2023, 3, 488−497

these metrics can be used to identify high-performing materials.

Figure 3 shows the categorization of QMOFs in four regions with respect to their $R\%_{C4H10,quat}$ and $APS_{C4H10,quat}$. In the low

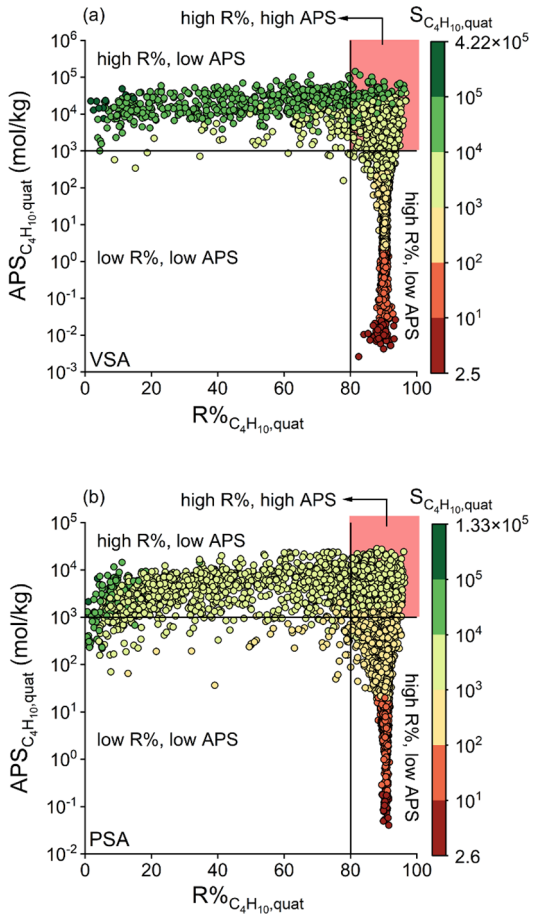

Figure 3. Calculated $APS_{C4H10,quat}$ and $R\%_{C4H10,quat}$ of 3,496 QMOF adsorbents for the separation of C_4H_{10} from the quaternary air mixture at (a) VSA and (b) PSA conditions. Data points were colored based on $S_{C4H10,quat}$ at 1 and 10 bar, respectively.

$R\%_{C4H10,quat}$ (<80%)-low $APS_{C4H10,quat}$ (<10^3 mol/kg) region, there are 10 (154) QMOFs at VSA (PSA) condition, considered to be unpromising. In the low $R\%_{C4H10,quat}$–high $APS_{C4H10,quat}$ region, there are 567 (1,044) QMOFs for the VSA (PSA) process, exhibiting $APS_{C4H10,quat}$ > 10^3 mol/kg but suffering from low $R\%_{C4H10,quat}$ values (<80%). Since regenerating the adsorbents is important for the economic efficiency of the separation processes, these QMOFs were also considered to be potentially unpromising. In the high $R\%_{C4H10,quat}$–low $APS_{C4H10,quat}$ region, a total of 2,306 (1,652) QMOFs were identified at VSA (PSA) condition, achieving sufficiently high $R_{C4H10,quat}$ values (>80%) but with relatively low $APS_{C4H10,quat}$ (<10^3 mol/kg). In the high $R\%_{C4H10,quat}$–high $APS_{C4H10,quat}$ region (red region), 613 (646) QMOFs exist for the VSA (PSA) process with $R\%_{C4H10,quat}$ > 80% and $APS_{C4H10,quat}$ > 10^3 mol/kg, and these are promising adsorbent candidates for VOC capture from a mixture of N_2, O_2, Ar, and C_4H_{10}.

To identify the structural features leading to adsorbents having different $R\%_{C4H10,quat}$–$APS_{C4H10,quat}$ combinations, we investigated the relationship between the structural properties and separation performances of QMOFs. Figures S3 and S4 demonstrate the impact of the PLD, ϕ, and S_{acc} on the performance of QMOFs at VSA and PSA conditions, respectively. Generally, QMOFs with narrow PLD (5−10 Å), low ϕ (0.3−0.6), and low S_{acc} (146−1,000 m^2/g) exhibit high selectivities (>10^3) at 1 bar, as depicted in Figure S3a,b along with a moderate $\Delta N_{C_4H_{10},quat}$ (up to 2 mol/kg), as shown in Figure S3c,d at VSA condition. QMOFs achieving $APS_{C4H10,quat}$ > 10^3 mol/kg at VSA condition typically possess PLD < 15 Å, ϕ < 0.8, and S_{acc} < 4,000 m^2/g, as shown in Figure S3e,f. There is no distinct trend between $R\%$ and structural properties, except that QMOFs with S_{acc} > 4,000 m^2/g mostly exhibit an $R\%$ > 80%, as observed in Figure S3g,h. QMOFs achieving $APS_{C4H10,quat}$ > 10^3 mol/kg with an $R\%_{C4H10,quat}$ > 80% at VSA condition have PLD, ϕ, and S_{acc} values in between 5 and 15 Å, 0.4−0.8, and 297−3,812 m^2/g, respectively. Similarly, as illustrated in Figure S4, QMOFs possessing PLD in the range of 5−15 Å, ϕ between 0.5 and 0.8, and S_{acc} between 508 and 4,631 m^2/g tend to exhibit $APS_{C4H10,quat}$ > 10^3 mol/kg and $R\%_{C4H10,quat}$ > 80% at PSA conditions. Overall, structures with narrow pores and moderate porosities enable the efficient confinement of C_4H_{10} molecules within the pores, resulting in a higher $S_{C4H10,quat}$ and $APS_{C4H10,quat}$.

Until this point, we assessed the VOC capture performances of QMOFs considering that the air mixture is pre-dried. However, water vapor may be present in the air mixture and compete with VOCs for adsorption in MOFs.[28] Therefore, before proceeding with the more realistic seven-component mixture simulations, we identified the hydrophobic QMOFs by computing $K_{H,H2O}$ values of the promising QMOFs offering $R\%_{C4H10,quat}$ > 80% and $APS_{C4H10,quat}$ > 10^3 mol/kg. Thirty-seven QMOFs were classified as hydrophobic since they have $K_{H,H2O}$ values of <2.5 × 10^{-6} mmol/g/Pa. Most of the QMOFs identified to have a very high $APS_{C4H10,quat}$ were found to be hydrophilic ($K_{H,H2O}$ > 2.5 × 10^{-6} mmol/g/Pa), and they were eliminated. The 37 promising QMOFs were further studied for the adsorption-based separation of C_4H_{10} from a more realistic seven-component air mixture, that is, $N_2/O_2/Ar/C_4H_{10}/C_3H_8/C_3H_6/C_2H_6$. Figure 4a,b shows the C_4H_{10} selectivities ($S_{C4H10,7-comp}$) and working capacities ($\Delta N_{C_4H_{10},7-comp}$) of the 37 promising QMOFs obtained for the separation of the seven-component air mixture at VSA and PSA conditions. The seven-component butane selectivities and working capacities of 37 QMOFs were calculated in between 596 and 9 × 10^3 (637−5.6 × 10^3) and 0.03−0.45 (0.23−1.45) mol/kg at VSA (PSA) condition, respectively.

We also calculated $APS_{C4H10,7-comp}$ of 37 QMOFs in between 17.9 and 3.6 × 10^3 mol/kg (226−7.5 × 10^3 mol/kg) at VSA (PSA) condition. Blue curves in Figure 4a,b denote an $APS_{C4H10,7-comp}$ of 10^3 mol/kg as an upper bound for identifying the most promising materials. There are six (23) QMOFs that can exceed the upper bound at VSA (PSA) conditions. We note that APSs of QMOFs computed for the separation of the seven-component air mixture were lower than those computed for the separation of a quaternary mixture. This can be explained by the lower C_4H_{10} working capacities both at VSA and PSA conditions due to the competitive adsorption between C_4H_{10} and other VOC molecules (C_3H_8, C_3H_6, and C_2H_6) in the seven-component mixture. Figure 4c,d represents the classification of QMOFs based on $R\%_{C4H10,7-comp}$ and $APS_{C4H10,7-comp}$ under VSA and PSA conditions. All

https://doi.org/10.1021/acsengineeringau.3c00039
ACS Eng. Au 2023, 3, 488−497

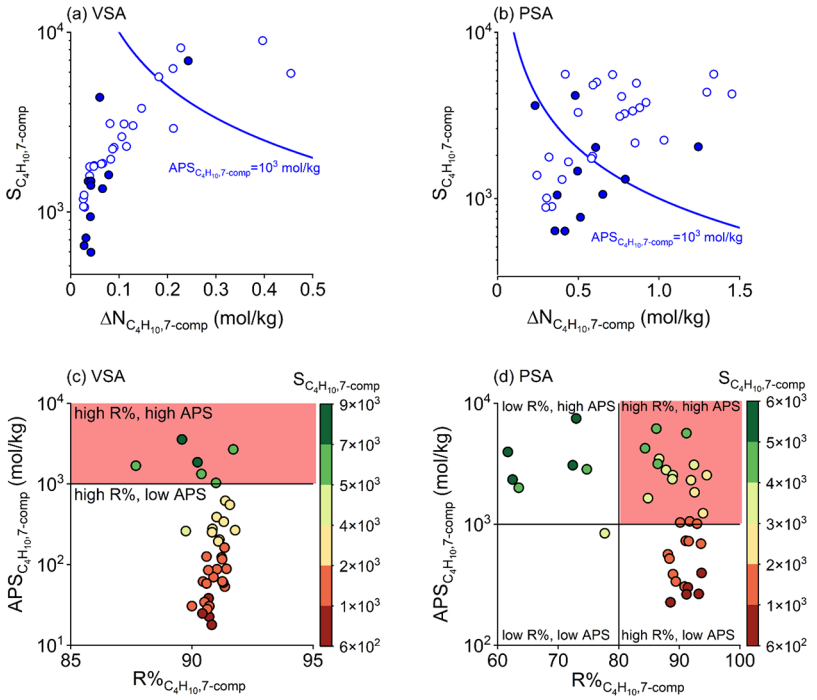

Figure 4. Butane selectivities and working capacities of 37 promising QMOFs for the separation of a seven-component air mixture calculated at (a) VSA and (b) PSA conditions. Closed (open) symbols represent synthesized (hypothetical) QMOFs. Calculated $APS_{C4H10,7\text{-comp}}$ and $R\%_{C4H10,7\text{-comp}}$ of QMOFs under (c) VSA and (d) PSA conditions. Data points in (c) and (d) were colored based on $S_{C4H10,7\text{-comp}}$ at 1 and 10 bar, respectively.

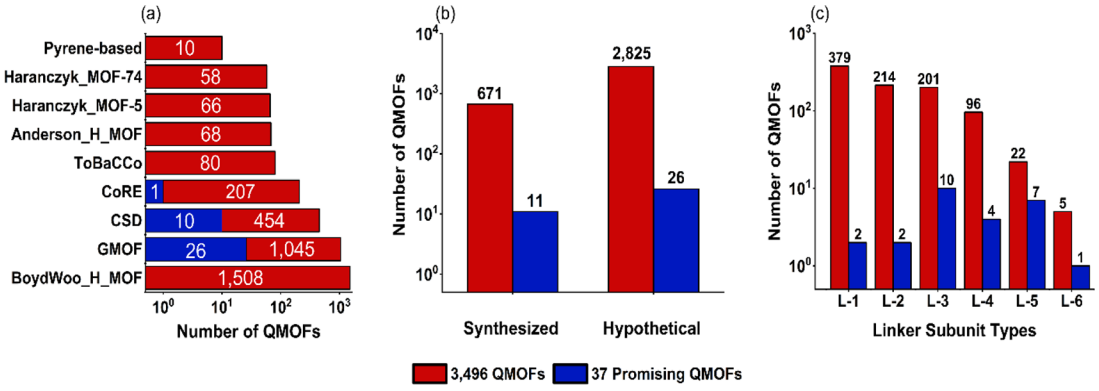

Figure 5. (a) Number of QMOFs retrieved from each MOF database, (b) number of synthesized and hypothetical QMOFs, and (c) number of QMOFs that contain L1-L6 linker subunits. The red column represents the QMOFs in the initial set of 3,496 QMOFs and blue column represents QMOFs in the final set of 37 promising QMOFs.

QMOFs offered high $R\%_{C4H10,7\text{-comp}}$ values between 88 and 92% at VSA condition. In contrast, $R\%_{C4H10,7\text{-comp}}$ values vary between 62 and 95%, and six QMOFs with $APS_{C4H10,7\text{-comp}} > 10^3$ mol/kg suffer from moderate $R\%_{C4H10,7\text{-comp}}$ values (62−75%) at PSA condition. The high $APS_{C4H10,7\text{-comp}}$ of QMOFs having an $R\%_{C4H10,7\text{-comp}} > 80\%$ can be attributed to their high $S_{C4H10,7\text{-comp}}$ ($>5.0 \times 10^3$ (1.0×10^3) at VSA (PSA) condition), as indicated by the red region in Figure 4c,d.

We then investigated structural and chemical properties of the top-performing QMOFs for the separation of C_4H_{10} from the seven-component air mixture. Figure 5 illustrates the distribution of the materials' characteristics in our initial set composed of 3,496 QMOFs and 37 promising QMOFs that we identified after computational screening of the initial set. Figure 5a demonstrates that QMOFs in our initial set were collected from nine distinct MOF databases, while the 37 promising QMOFs were sourced from only three different databases, namely, CoRE, CSD, and GMOF, and most of these structures were from the hypothetical GMOF database,[21] consisting of more than 300,000 materials. Figure 5b shows that the initial set of 3,496 QMOFs and the 37 promising QMOFs exhibit similar distributions concerning the number of synthesized and hypothetical structures, and the majority in both sets comprises the hypothetical structures. Previous studies emphasized the substantial influence of the type of linkers and metal nodes of MOFs on their adsorption properties for linear C_4-C_6 alkanes and their isomers.[64] To focus on these features, we identified the top five QMOFs, which offered the highest $APS_{C4H10,7\text{-comp}}$ with $R\%_{C4H10,7\text{-comp}} > 80\%$ at VSA and PSA conditions, as listed in Table S2. Six different linker subunits, shown in Table S1, were identified in these top QMOFs. We searched through our initial set of 3,496 QMOFs and the set of 37 promising QMOFs for these linker subunit types and presented their distribution in Figure

https://doi.org/10.1021/acsengineeringau.3c00039
ACS Eng. Au 2023, 3, 488−497

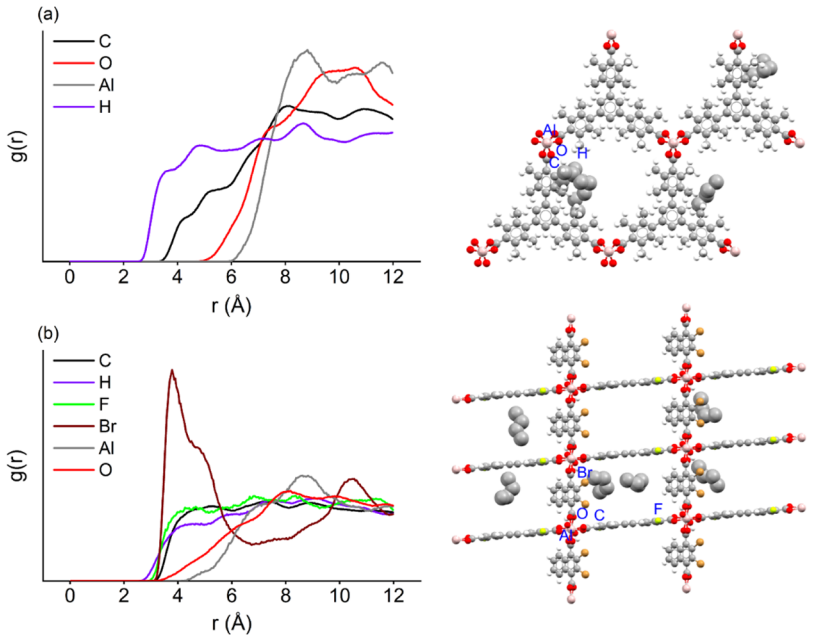

Figure 6. RDF plots and snapshots of C_4H_{10} molecules generated at 1 bar and 298 K for the separation of a seven-component air mixture with (a) qmof-d9ca2be and (b) qmof-7559c55. Gray, white, red, orange, green, and rose spheres represent C, H, O, Br, F, and Al atoms, respectively. Butane molecules are shown with gray space-filled models.

5c. Labeling of linker subunits as L-1 to L-6 was made based on the occurrence frequency of these linkers in our initial QMOF set: L-1:4,4′-(1,2-ethynediyl)dibenzoic acid, L-2:1,4-naphthalenedicarboxylic acid, L-3: bicyclo[4.2.0]octa-1,3,5-triene-2,5-dicarboxylic acid, L-4:1,3,5-tris(4-carboxyphenyl)-benzene, L-5:2,4,6-tris(4-carboxyphenyl)-1,3,5-triazine, and L-6:3-(2-pyridyl)-5-(4-pyridyl)-1,2,4-triazole. For example, L-1 was found in 379 of the QMOFs but L-6 was found in only five of the QMOFs in the initial set, as shown in red columns in Figure 5c.

We found at least one of the L1-L6 linker subunits in 845 structures among 3,496 QMOFs in our initial set, while for the set of 37 promising QMOFs, at least one of these linkers was found in 24 distinct QMOFs. Among the set of promising QMOFs, 10 of them feature the linker subunit L-3, while linker subunits L-1 to L-5 are present in 23 QMOFs derived from the hypothetical GMOF database. L-6, which contains a triazolate group, is unique to a QMOF that has been obtained from the CSD database. As shown in Table S1, linker subunits of L-1 to L-6 feature aromatic rings, while linker subunits L-1 to L-5 additionally contain carboxylic acid groups. These results from the analysis of high-performance materials are in good agreement with experimental reports on the potential of MOFs containing aromatic rings for VOC separation.[32,65]

The interaction with the metal site and the accessibility of the metal site are also important factors for the adsorption of VOCs.[30] Figure S5 indicates the distribution of linker subunit types, topologies, and metal types in the set of 37 promising QMOFs. Among 38 metal types and 87 topologies reported in our initial set,[33,34] Al metal and *tsg* topology together with an L-1 linker are the most frequently observed properties in the 37 promising QMOFs. The top QMOFs have two different metals (alumina (Al) and cobalt (Co)) and four different topologies (*tsg*, *ttp*, *rna*, and *nbo*) as shown in Table S2. Finally, the top QMOFs have PLDs of 6−9 Å, ϕ of 0.4−0.6, and S_{acc} < ∼1,300 m^2/g. We note that these structural and chemical properties are important, but they alone are not sufficient for a QMOF to be identified as a top adsorbent for C_4H_{10} separation since the overall performance of a material is influenced by a combination of various properties, and the presence of other VOCs competing for the available adsorption sites also impacts the materials' performance.

We finally investigated the preferential adsorption sites of the top two QMOFs, namely, qmof-d9ca2be and qmof-7559c55, offering the highest $APS_{C4H10,7\text{-comp}}$ together with $R\%_{C4H10,7\text{-comp}}$ > 80% for VSA and PSA processes, respectively, by performing RDF analysis at 1 bar, 298 K. Figure 6 illustrates that C_4H_{10} molecules tend to locate near the organic part of the QMOF structure. In both qmof-7559c55 and qmof-d9ca2be, H, which is found in the organic part of the QMOFs, is the first atom with which C_4H_{10} molecules interact. Figure 6a shows that C_4H_{10} molecules tend to locate ∼3 Å near H atoms in qmof-d9ca2be since the pore environment consists of H atoms of the methyl groups connected to organic linkers in this QMOF. Overall, these results indicate that C_4H_{10} molecules mostly prefer linker parts of the QMOFs as favorable adsorption sites. Figure 6b represents that C_4H_{10} molecules can be found within ∼3 Å distance to the linker atoms of qmof-7559c55, such as Br and F. The strongest peak belongs to the C_4H_{10} and Br interaction at an ∼4 Å distance, indicating that Br atoms provide the most favorable adsorption sites for C_4H_{10}.

We note that the accuracy and reliability of our computational work are defined by the validity of the assumptions we used. We assumed that all QMOFs will exhibit rigid behavior during gas adsorption, although it may not be valid for all MOFs, which may have breathing behavior upon exposure to an external stimuli such as pressure or temperature or upon adsorption of some gases.[66] We identified the top QMOFs for C_4H_{10} capture from a realistic seven-component air mixture, and the stability and synthesizability of these materials need to be further studied to use them in real applications. For example, one of the top QMOFs that we identified was already synthesized (qmof-4b1ef88, reported as BUSMUY in CSD)[65]

https://doi.org/10.1021/acsengineeringau.3c00039
ACS Eng. Au 2023, 3, 488−497

and reported to be thermally stable until 643 K in the air environment, which exceeds the temperature we studied, that is, 298 K. Several of the top QMOFs identified in this work are hypothetical and subjected to further experimental investigation. However, considering that most of the linkers and metal nodes utilized in constructing these hypothetical structures have been experimentally observed in existing MOFs,[21] their synthesis through novel synthetic approaches would be feasible. Finally, we would like to emphasize that the intracrystalline diffusivity of gas molecules was negligible[66] in our approach of using CBMC simulations for studying gas adsorption behavior of MOFs at equilibrium at the atomic scale. In the future steps of evaluating the most promising adsorbent candidates, kinetic effects and diffusional constraints resulting from the difference in the intracrystalline diffusivity of gas molecules during adsorption in a fixed bed can studied.[67,68] This involves utilizing process modeling tools to further analyze the effect of design parameters such as the MOF pellet size and orientation, column length and diameter, bed height, and packing density at the macro scale to minimize or eliminate diffusional limitations in the separation columns filled with adsorbents. We believe that further studies considering these effects and identifying design parameters for modeling an adsorption column filled with high-performing MOFs would be of utmost importance in future research.

4. CONCLUSIONS

In this study, we examined a total of 3,496 different experimental and hypothetical QMOFs for selective capture of C_4H_{10} from ambient air at VSA and PSA conditions using CBMC simulations. Selectivities reaching a maximum of 4.2×10^5 (1.3×10^5) at 1 bar (10 bar) and working capacities reaching 4.6 (6.8) mol/kg at VSA (PSA) conditions were computed for the separation of C_4H_{10} from a quaternary $N_2/O_2/Ar/C_4H_{10}$ mixture, leading to 1,180 (1,691) QMOFs with $APS_{C4H10,quat}$ higher than 10^3 mol/kg at VSA (PSA) conditions. A total of 1,403 and 1,514 QMOFs were shown to have superior C_4H_{10} selectivity than the famous zeolite MFI at 1 and 10 bar, respectively. Thirty-seven promising QMOFs, which comply with the criteria of $R\%_{C4H10,quat} > 80\%$ and $APS_{C4H10,quat} > 10^3$ mol/kg and are also hydrophobic, were further studied for the separation of C_4H_{10} from a more realistic seven-component $N_2/O_2/Ar/C_4H_{10}/C_3H_8/C_3H_6/C_2H_6$ mixture. They were computed to have butane selectivities in the range of $596–9 \times 10^3$ at 1 bar (between 637 and 5.6×10^3 at 10 bar) and their working capacities varied between 0.03 and 0.45 mol/kg (0.23–1.45) at VSA (PSA) conditions. The detailed investigation of structural, chemical, and topological properties using different computational tools highlighted that the low porosity (0.4–0.6), narrow pore sizes (6–9 Å), presence of linker subunits containing aromatic rings, Al and Co metal sites, and *tsg*, *ttp*, *rna*, and *nbo* topologies are the common features of the high-performing QMOFs. The hierarchical computational screening methodology that we proposed and used in this study will guide the design and discovery of new MOFs specifically tailored for direct C_4H_{10} capture from air.

■ ASSOCIATED CONTENT

Supporting Information

The Supporting Information is available free of charge at https://pubs.acs.org/doi/10.1021/acsengineeringau.3c00039.

Comparison of simulation results for N_2, O_2, Ar, and C_4H_{10} uptakes obtained with a total of 10^5 and 10^6 cycles; comparison of gas uptakes obtained from the literature and our simulation results for single C_4H_{10} and an equimolar mixture (C_4H_{10}/C_4H_8 and C_3H_8/C_3H_6) adsorption at 0.1, 1, 10 bar; relation between performance metrics ($S_{C4H10,quat}$, $\Delta N_{C4H10,quat}$, $APS_{C4H10,quat}$, and $R\%_{C4H10,quat}$) and structural properties (PLD, ϕ, and S_{acc}) at VSA and PSA conditions; analysis of metal types, linker subunits, and topologies of high-performing materials for the separation of the seven-component mixture at PSA and VSA conditions; illustration of linker subunit and topology types; structural properties and performance metrics for top five QMOFs at VSA and PSA conditions, and a list of linker subunits (PDF)

■ AUTHOR INFORMATION

Corresponding Author

Seda Keskin − *Department of Chemical and Biological Engineering, Koc University, 34450 Istanbul, Turkey;* orcid.org/0000-0001-5968-0336; Phone: +90 (212) 338-1362; Email: skeskin@ku.edu.tr

Authors

Goktug Ercakir − *Department of Chemical and Biological Engineering, Koc University, 34450 Istanbul, Turkey*

Gokhan Onder Aksu − *Department of Chemical and Biological Engineering, Koc University, 34450 Istanbul, Turkey;* orcid.org/0000-0002-0128-4776

Cigdem Altintas − *Department of Chemical and Biological Engineering, Koc University, 34450 Istanbul, Turkey*

Complete contact information is available at: https://pubs.acs.org/10.1021/acsengineeringau.3c00039

Author Contributions

CRediT: **Goktug Ercakir** investigation, methodology, writing-original draft, writing-review & editing; **Gokhan Onder Aksu** investigation, methodology, writing-review & editing; **Cigdem Altintas** investigation, methodology, writing-review & editing; **Seda Keskin** conceptualization, investigation, methodology, resources, writing-original draft, writing-review & editing.

Notes

The authors declare no competing financial interest.

■ ACKNOWLEDGMENTS

S.K. acknowledges ERC-2017-Starting Grant. This study has received funding from the European Research Council (ERC) under the European Union's Horizon 2020 research and innovation programme (ERC-2017-Starting Grant, grant agreement no. 756489-COSMOS). The authors declare no competing financial interest. Authors thank to Dr. Hakan Demir for fruitful discussion.

■ REFERENCES

(1) Zhang, F.; Shi, Y.; Fang, D.; Ma, G.; Nie, C.; Krafft, T.; He, L.; Wang, Y. Monitoring History and Change Trends of Ambient Air Quality in China During the Past Four Decades. *J. Environ. Manage.* **2020**, *260*, No. 110031.

(2) Konkle, S. L.; Zierold, K. M.; Taylor, K. C.; Riggs, D. W.; Bhatnagar, A. National Secular Trends in Ambient Air Volatile Organic Compound Levels and Biomarkers of Exposure in the United States. *Environ. Res.* **2020**, *182*, No. 108991.

(3) Sicard, P.; Agathokleous, E.; De Marco, A.; Paoletti, E.; Calatayud, V. Urban Population Exposure to Air Pollution in Europe over the Last Decades. *Environ. Sci. Eur.* **2021**, *33* (1), 28.
(4) Sheoran, K.; Siwal, S. S.; Kapoor, D.; Singh, N.; Saini, A. K.; Alsanie, W. F.; Thakur, V. K. Air Pollutants Removal Using Biofiltration Technique: A Challenge at the Frontiers of Sustainable Environment. *ACS Eng. Au* **2022**, *2* (5), 378−396.
(5) Khan, F. I.; Ghoshal, A. K. Removal of Volatile Organic Compounds from Polluted Air. *J. Loss Prevent Proc.* **2000**, *13* (6), 527−545.
(6) Li, X. Q.; Zhang, L.; Yang, Z. Q.; Wang, P.; Yan, Y. F.; Ran, J. Y. Adsorption Materials for Volatile Organic Compounds (VOCs) and the Key Factors for VOCs Adsorption Process: A Review. *Sep. Purif. Technol.* **2020**, *235*, No. 116213.
(7) Siu, B.; Chowdhury, A. R.; Yan, Z. W.; Humphrey, S. M.; Hutter, T. Selective Adsorption of Volatile Organic Compounds in Metal-Organic Frameworks (MOFs). *Coord. Chem. Rev.* **2023**, *485*, No. 215119.
(8) Furukawa, H.; Cordova, K. E.; O'Keeffe, M.; Yaghi, O. M. The Chemistry and Applications of Metal-Organic Frameworks. *Science* **2013**, *341* (6149), 1230444.
(9) Xiang, Z.; Peng, X.; Cheng, X.; Li, X.; Cao, D. CNT@$Cu_3(BTC)_2$ and Metal−Organic Frameworks for Separation of CO_2/CH_4 Mixture. *J. Phys. Chem. C* **2011**, *115* (40), 19864−19871.
(10) Kumar, P.; Kim, K. H.; Kwon, E. E.; Szulejko, J. E. Metal-Organic Frameworks for the Control and Management of Air Quality: Advances and Future Direction. *J. Mater. Chem. A* **2016**, *4* (2), 345−361.
(11) Edubilli, S.; Gumma, S. A Systematic Evaluation of UiO-66 Metal Organic Framework for CO_2/N_2 Separation. *Sep. Purif. Technol.* **2019**, *224*, 85−94.
(12) Severino, M. I.; Al Mohtar, A.; Soares, C. V.; Kolmykov, O.; Freitas, C.; Dovgaliuk, I.; Martineau, C.; Pimenta, V.; Nouar, F.; Maurin, G.; et al. Hydrophobic MOFs for the Efficient Capture of Highly Polar Volatile Organic Compound. *J. Mater. Chem. A* **2023**, *11* (8), 4238−4247.
(13) Li, Y.-Z.; Wang, G.-D.; Shi, W.-J.; Hou, L.; Wang, Y.-Y.; Zhu, Z. Efficient C_2H_n Hydrocarbons and VOC Adsorption and Separation in an MOF with Lewis Basic and Acidic Decorated Active Sites. *ACS Appl. Mater. Interfaces* **2020**, *12* (37), 41785−41793.
(14) González-Galán, C.; De Fez-Febré, M.; Giancola, S.; González-Cobos, J.; Vidal-Ferran, A.; Galán-Mascarós, J. R.; Balestra, S. R. G.; Calero, S. Separation of Volatile Organic Compounds in TAMOF-1. *ACS Appl. Mater. Interfaces* **2022**, *14* (27), 30772−30785.
(15) Groom, C. R.; Bruno, I. J.; Lightfoot, M. P.; Ward, S. C. The Cambridge Structural Database. *Acta Crystallogr., Sect. B: Struct. Sci., Cryst. Eng. Mater.* **2016**, *72* (2), 171−179.
(16) Moghadam, P. Z.; Li, A.; Wiggin, S. B.; Tao, A.; Maloney, A. G. P.; Wood, P. A.; Ward, S. C.; Fairen-Jimenez, D. Development of a Cambridge Structural Database Subset: A Collection of Metal-Organic Frameworks for Past, Present, and Future. *Chem. Mater.* **2017**, *29* (7), 2618−2625.
(17) Chung, Y. G.; Camp, J.; Haranczyk, M.; Sikora, B. J.; Bury, W.; Krungleviciute, V.; Yildirim, T.; Farha, O. K.; Sholl, D. S.; Snurr, R. Q. Computation-Ready, Experimental Metal-Organic Frameworks: A Tool To Enable High-Throughput Screening of Nanoporous Crystals. *Chem. Mater.* **2014**, *26* (21), 6185−6192.
(18) Chung, Y. G.; Haldoupis, E.; Bucior, B. J.; Haranczyk, M.; Lee, S.; Zhang, H. D.; Vogiatzis, K. D.; Milisavljevic, M.; Ling, S. L.; Camp, J. S.; et al. Advances, Updates, and Analytics for the Computation-Ready, Experimental Metal-Organic Framework Database: CoRE MOF 2019. *J. Chem. Eng. Data* **2019**, *64* (12), 5985−5998.
(19) Boyd, P. G.; Chidambaram, A.; Garcia-Diez, E.; Ireland, C. P.; Daff, T. D.; Bounds, R.; Gladysiak, A.; Schouwink, P.; Moosavi, S. M.; Maroto-Valer, M. M.; et al. Data-driven Design of Metal-Organic Frameworks for Wet Flue Gas CO_2 Capture. *Nature* **2019**, *576* (7786), 253−256.
(20) Boyd, P. G.; Woo, T. K. A Generalized Method for Constructing Hypothetical Nanoporous Materials of Any Net Topology from Graph Theory. *CrystEngComm* **2016**, *18* (21), 3777−3792.
(21) Lan, Y. S.; Yan, O. G.; Tong, M. M.; Zhong, C. L. Large-Scale Computational Assembly of Ionic Liquid/MOF Composites: Synergistic Effect in the Wire-Tube Conformation for Efficient CO_2/CH_4 Separation. *J. Mater. Chem. A* **2019**, *7* (20), 12556−12564.
(22) Colón, Y. J.; Gomez-Gualdron, D. A.; Snurr, R. Q. Topologically Guided, Automated Construction of Metal−Organic Frameworks and Their Evaluation for Energy-Related Applications. *Cryst. Growth Des.* **2017**, *17* (11), 5801−5810.
(23) Fernandez, M.; Boyd, P. G.; Daff, T. D.; Aghaji, M. Z.; Woo, T. K. Rapid and Accurate Machine Learning Recognition of High Performing Metal Organic Frameworks for CO_2 Capture. *J. Phys. Chem. Lett.* **2014**, *5* (17), 3056−3060.
(24) Majumdar, S.; Moosavi, S. M.; Jablonka, K. M.; Ongari, D.; Smit, B. Diversifying Databases of Metal Organic Frameworks for High-Throughput Computational Screening. *ACS Appl. Mater. Interfaces* **2021**, *13* (51), 61004−61014.
(25) Gómez-Gualdrón, D. A.; Colón, Y. J.; Zhang, X.; Wang, T. C.; Chen, Y.-S.; Hupp, J. T.; Yildirim, T.; Farha, O. K.; Zhang, J.; Snurr, R. Q. Evaluating Topologically Diverse Metal−Organic Frameworks for Cryo-Adsorbed Hydrogen Storage. *Energy Environ. Sci.* **2016**, *9* (10), 3279−3289.
(26) Daglar, H.; Gulbalkan, H. C.; Avci, G.; Aksu, G. O.; Altundal, O. F.; Altintas, C.; Erucar, I.; Keskin, S. Effect of Metal-Organic Framework (MOF) Database Selection on the Assessment of Gas Storage and Separation Potentials of MOFs. *Angew. Chem., Int. Ed. Engl.* **2021**, *60* (14), 7828−7837.
(27) Liu, Z.; Wang, X.; Liu, Y.; Li, L.; Li, S. Computational Screening of Metal-Organic Frameworks for Ammonia Capture from Humid Air. *Microporous Mesoporous Mater.* **2022**, *331*, No. 111659.
(28) Qiao, Z. W.; Xu, Q. S.; Jiang, J. W. Computational Screening of Hydrophobic Metal-Organic Frameworks for The Separation of H_2S and CO_2 from Natural Gas. *J. Mater. Chem. A* **2018**, *6* (39), 18898−18905.
(29) Gulcay-Ozcan, E.; Iacomi, P.; Rioland, G.; Maurin, G.; Devautour-Vinot, S. Airborne Toluene Detection Using Metal-Organic Frameworks. *ACS Appl. Mater. Interfaces* **2022**, *14* (48), 53777−53787.
(30) Liu, X.; Wang, R.; Wang, X.; Xu, D. High-Throughput Computational Screening and Machine Learning Model for Accelerated Metal−Organic Frameworks Discovery in Toluene Vapor Adsorption. *J. Phys. Chem. C* **2023**, *127* (23), 11268−11282.
(31) Yuan, X. Y.; Deng, X. M.; Cai, C. Z.; Shi, Z. N.; Liang, H.; Li, S. H.; Qiao, Z. W. Machine Learning and High-Throughput Computational Screening of Hydrophobic Metal-Organic Frameworks for Capture of Formaldehyde from Air. *Green Energy Environ.* **2021**, *6* (5), 759−770.
(32) Yuan, X.; Li, L.; Shi, Z.; Liang, H.; Li, S.; Qiao, Z. Molecular-Fingerprint Machine-Learning-Assisted Design and Prediction for High-Performance MOFs For Capture of NMHCs from Air. *Adv. Powder Mater.* **2022**, *1* (3), 100026.
(33) Rosen, A. S.; Iyer, S. M.; Ray, D.; Yao, Z. P.; Aspuru-Guzik, A.; Gagliardi, L.; Notestein, J. M.; Snurr, R. Q. Machine Learning the Quantum-Chemical Properties of Metal-Organic Frameworks for Accelerated Materials Discovery. *Matter-Us* **2021**, *4* (5), 1578−1597.
(34) Rosen, A. S.; Fung, V.; Huck, P.; O'Donnell, C. T.; Horton, M. K.; Truhlar, D. G.; Persson, K. A.; Notestein, J. M.; Snurr, R. Q. High-throughput predictions of metal−organic framework electronic properties: theoretical challenges, graph neural networks, and data exploration. *npj Comput. Mater.* **2022**, *8* (1), 112.
(35) Zhang, Z.; Zhang, C.; Zhang, Y.; Deng, S.; Yang, Y. F.; Su, A.; She, Y. B. Predicting Band Gaps of MOFs on Small Data by Deep Transfer Learning with Data Augmentation Strategies. *RSC Adv.* **2023**, *13* (25), 16952−16962.
(36) Moosavi, S. M.; Novotny, B. A.; Ongari, D.; Moubarak, E.; Asgari, M.; Kadioglu, O.; Charalambous, C.; Ortega-Guerrero, A.; Farmahini, A. H.; Sarkisov, L.; et al. A Data-Science Approach to

Predict The Heat Capacity of Nanoporous Materials. *Nat. Mater.* **2022**, *21* (12), 1419−1425.
(37) Willems, T. F.; Rycroft, C.; Kazi, M.; Meza, J. C.; Haranczyk, M. Algorithms and Tools for High-Throughput Geometry-Based Analysis of Crystalline Porous Materials. *Microporous Mesoporous Mater.* **2012**, *149* (1), 134−141.
(38) Tanaka, K.; Taguchi, A.; Hao, J.; Kita, H.; Okamoto, K. Permeation and Separation Properties of Polyimide Membranes to Olefins and Paraffins. *J. Membr. Sci.* **1996**, *121* (2), 197−207.
(39) Sircar, S. Basic Research Needs for Design of Adsorptive Gas Separation Processes. *Ind. Eng. Chem. Res.* **2006**, *45* (16), 5435−5448.
(40) Dubbeldam, D.; Torres-Knoop, A.; Walton, K. S. On the Inner Workings of Monte Carlo Codes. *Mol. Simul.* **2013**, *39* (14−15), 1253−1292.
(41) Dubbeldam, D.; Calero, S.; Ellis, D. E.; Snurr, R. Q. RASPA: Molecular Simulation Software for Adsorption and Diffusion in Flexible Nanoporous Materials. *Mol. Simul.* **2016**, *42* (2), 81−101.
(42) Calero, S.; Gomez-Alvarez, P. On The Performance of FAU and MFI Zeolites for the Adsorptive Removal of A Series of Volatile Organic Compounds from Air Using Molecular Simulation. *Phys. Chem. Chem. Phys.* **2015**, *17* (39), 26451−26455.
(43) Martin, M. G.; Siepmann, J. I. Transferable Potentials for Phase Equilibria. 1. United-Atom Description of n-Alkanes. *J. Phys. Chem. B* **1998**, *102* (14), 2569−2577.
(44) Potoff, J. J.; Siepmann, J. I. Vapor-Liquid Equilibria of Mixtures Containing Alkanes, Carbon Dioxide, and Nitrogen. *AIChE J.* **2001**, *47* (7), 1676−1682.
(45) Zhang, L.; Siepmann, J. I. Direct Calculation of Henry's Law Constants from Gibbs Ensemble Monte Carlo Simulations: Nitrogen, Oxygen, Carbon Dioxide and Methane in Ethanol. *Theor. Chem. Acc.* **2006**, *115* (5), 391−397.
(46) Eggimann, B. L.; Sun, Y.; DeJaco, R. F.; Singh, R.; Ahsan, M.; Josephson, T. R.; Siepmann, J. I. Assessing the Quality of Molecular Simulations for Vapor−Liquid Equilibria: An Analysis of the TraPPE Database. *J. Chem. Eng. Data* **2020**, *65* (3), 1330−1344.
(47) García-Pérez, E.; Parra, J.; Ania, C. O.; Dubbeldam, D.; Vlugt, T. J.; Castillo, J.; Merkling, P.; Calero, S. Unraveling the Argon Adsorption Processes in MFI-type Zeolite. *J. Phys. Chem. C* **2008**, *112* (27), 9976−9979.
(48) Mayo, S. L.; Olafson, B. D.; Goddard, W. A. Dreiding - A Generic Force-Field for Molecular Simulations. *J. Phys. Chem-Us* **1990**, *94* (26), 8897−8909.
(49) Rappé, A. K.; Casewit, C. J.; Colwell, K.; Goddard, W. A., III; Skiff, W. M. UFF, A Full Periodic Table Force Field for Molecular Mechanics and Molecular Dynamics Simulations. *J. Am. Chem. Soc.* **1992**, *114* (25), 10024−10035.
(50) Ewald, P. P. Evaluation of Optical and Electrostatic Lattice Potentials. *Ann. Phys.* **1921**, *369* (3), 253−287.
(51) Manz, T. A.; Limas, N. G. Introducing DDEC6 Atomic Population Analysis: Part 1. Charge Partitioning Theory and Methodology. *RSC Adv.* **2016**, *6* (53), 47771−47801.
(52) Limas, N. G.; Manz, T. A. Introducing DDEC6 Atomic Population Analysis: Part 2. Computed Results for A Wide Range of Periodic and Nonperiodic Materials. *RSC Adv.* **2016**, *6* (51), 45727−45747.
(53) Daglar, H.; Keskin, S. Recent Advances, Opportunities, and Challenges in High-Throughput Computational Screening of MOFs for Gas Separations. *Coord. Chem. Rev.* **2020**, *422*, No. 213470.
(54) Jiang, J.; Sandler, S. I. Monte Carlo Simulation for the Adsorption and Separation of Linear and Branched Alkanes in IRMOF-1. *Langmuir* **2006**, *22* (13), 5702−5707.
(55) Luna-Triguero, A.; Vicent-Luna, J. M.; Gomez-Alvarez, P.; Calero, S. Olefin/Paraffin Separation in Open Metal Site Cu-BTC Metal-Organic Framework. *J. Phys. Chem. C* **2017**, *121* (5), 3126−3132.
(56) Gkourras, A.; Gergidis, L. N. Molecular and Artificial Neural Networks Modeling of Sorption and Diffusion of Small Alkanes, Alkenes and Their Ternary Mixtures in ZIF-8 at Different Temperatures. *J. Phys. Chem. B* **2022**, *126* (29), 5582−5594.
(57) Moghadam, P. Z.; Fairen-Jimenez, D.; Snurr, R. Q. Efficient Identification of Hydrophobic MOFs: Aapplication in the Capture of Toxic Industrial Chemicals. *J. Mater. Chem. A* **2016**, *4* (2), 529−536.
(58) Khalak, Y.; Baumeier, B.; Karttunen, M. Improved General-Purpose Five-Point Model for Water: TIP5P/2018. *J. Chem. Phys.* **2018**, *149* (22), 224507.
(59) Wei, W.; Lv, Z.; Yang, G.; Cheng, S.; Li, Y.; Wang, L. VOCs Emission Rate Estimate for Complicated Industrial Area Source Using An Inverse-Dispersion Calculation Method: A Case Study on a Petroleum Refinery in Northern China. *Environ. Pollut.* **2016**, *218*, 681−688.
(60) Wei, W.; Cheng, S. Y.; Li, G. H.; Wang, G.; Wang, H. Y. Characteristics of Volatile Organic Compounds (VOCs) Emitted from A Petroleum Refinery in Beijing, China. *Atmos. Environ.* **2014**, *89*, 358−366.
(61) Na, K.; Kim, Y. P.; Moon, K. C.; Moon, I.; Fung, K. Concentrations of Volatile Organic Compounds in An Industrial Area of Korea. *Atmos. Environ.* **2001**, *35* (15), 2747−2756.
(62) Yang, B.; Hawley, D.; Yao, J.; May, C.; Mendez-Arroyo, J. E.; Ess, D. H. Demonstration of High-Throughput Building Block and Composition Analysis of Metal-Organic Frameworks. *J. Chem. Inf. Model* **2022**, *62* (19), 4672−4679.
(63) Macrae, C. F.; Sovago, I.; Cottrell, S. J.; Galek, P. T. A.; McCabe, P.; Pidcock, E.; Platings, M.; Shields, G. P.; Stevens, J. S.; Towler, M.; et al. Mercury 4.0: From Visualization to Analysis, Design and Prediction. *J. Appl. Crystallogr.* **2020**, *53* (Pt 1), 226−235.
(64) Zhang, L.; Wang, Q.; Wu, T.; Liu, Y. C. Understanding Adsorption and Interactions of Alkane Isomer Mixtures in Isoreticular Metal-Organic Frameworks. *Chem. - Eur. J.* **2007**, *13* (22), 6387−6396.
(65) Tang, H.; Jiang, J. In Silico Screening and Design Strategies of Ethane-Selective Metal−Organic Frameworks for Ethane/Ethylene Separation. *AlChE J.* **2021**, *67* (3), No. e17025.
(66) Chang, Z.; Yang, D. H.; Xu, J.; Hu, T. L.; Bu, X. H. Flexible Metal-Organic Frameworks: Recent Advances and Potential Applications. *Adv. Mater.* **2015**, *27* (36), 5432−5441.
(67) Krishna, R. Highlighting the Influence of Thermodynamic Coupling on Kinetic Separations with Microporous Crystalline Materials. *ACS Omega* **2019**, *4* (2), 3409−3419.
(68) Krishna, R. Metrics for Evaluation and Screening of Metal−Organic Frameworks for Applications in Mixture Separations. *ACS Omega* **2020**, *5* (28), 16987−17004.

https://doi.org/10.1021/acsengineeringau.3c00039
ACS Eng. Au 2023, 3, 488−497